

Lunar OH/H₂O: Distribution, Variations, Origin and Mobility

JEAN-PHILIPPE COMBE

THOMAS B. MCCORD



New Approaches to Lunar Ice Detection and Mapping
1st Workshop
Keck Institute of Space Studies
California Institute of Technology, Pasadena, CA, USA
July 22nd, 2013

Lunar OH/H₂O

Distribution

Variations

Origins

Mobility

Lunar OH/H₂O Distribution

Prior to the observations: Models for the presence of **OH and H₂O in polar permanently cold areas**
(*Watson et al., 1961, JGR*)

Elemental hydrogen detected by neutron detectors

OH/H₂O detected with ultraviolet and near-infrared spectroscopy

Possible distinction between OH and H₂O with near-infrared spectroscopy

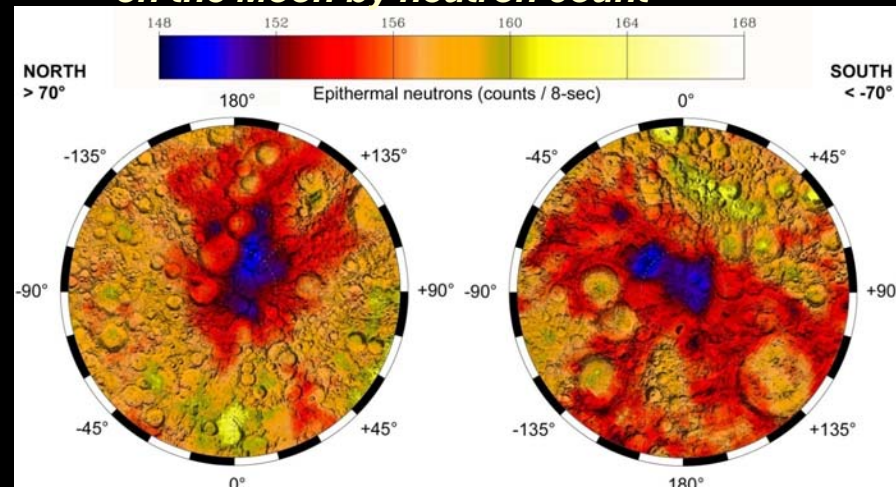
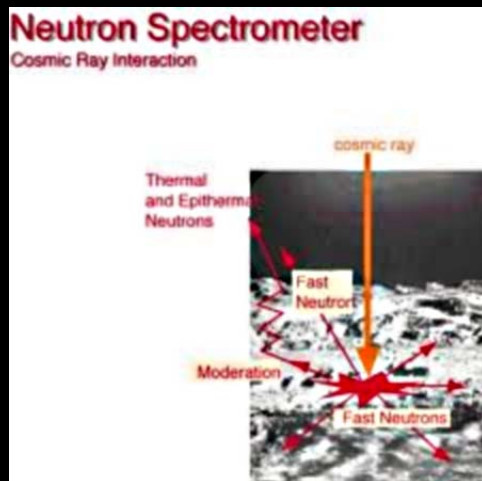
Mapping of Elemental Hydrogen and OH/H₂O

Distribution of Lunar OH/H₂O

Lunar Surface Elemental Hydrogen

Presence of H within the first meter below the surface, enrichment of the poles
Lunar Prospector (*Feldman et al., 1998 ; 2000*)

→ *First detection of elemental Hydrogen on the Moon by neutron count*



Galactic cosmic rays (GCRs)

- Reactions with the nuclear constituents of near-surface material → Neutrons of high energies (several hundred keV)
- Multiple elastic and inelastic collisions, scattering → Neutrons of lower energies (thermal and epithermal range)

Measured neutron fluxes

- Rate of production depend on
 - The incident flux of GCRs
 - The relative abundances of certain elements such as Fe and Ti
- Rate of absorption is determined mostly by the relative abundances of Fe, Ti, Gd, and Sm [*Lingenfelteert et al., 1972*].
- Rate of energy loss is determined mostly by the abundance of elemental hydrogen → The more hydrogen that is present, the faster is the rate of energy loss, which establishes a reduced flux of epithermal neutrons.

Distribution of Lunar OH/H₂O

Near-infrared spectroscopy of Lunar OH/H₂O

Laboratory measurements on lunar analogs
Hibbitts et al., 2011, Icarus 213

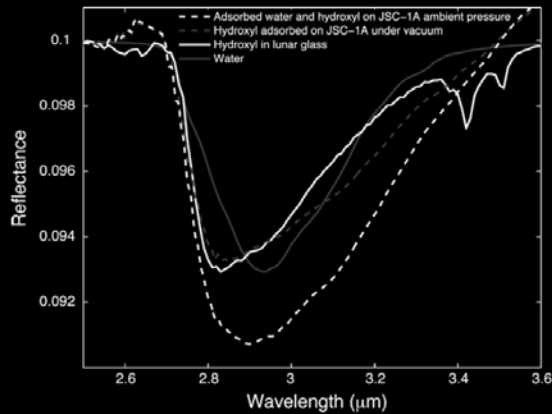
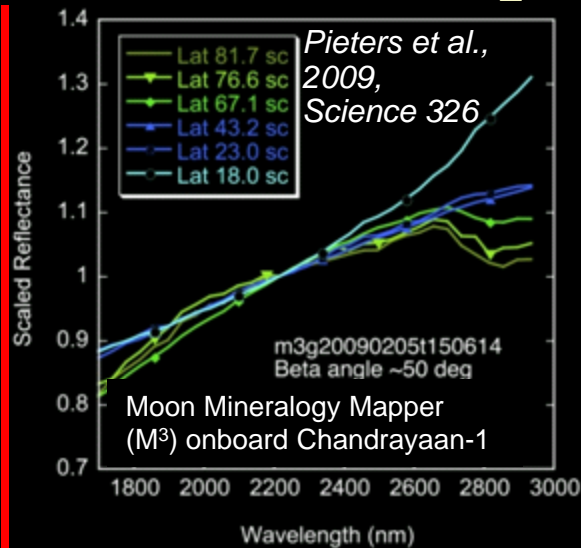
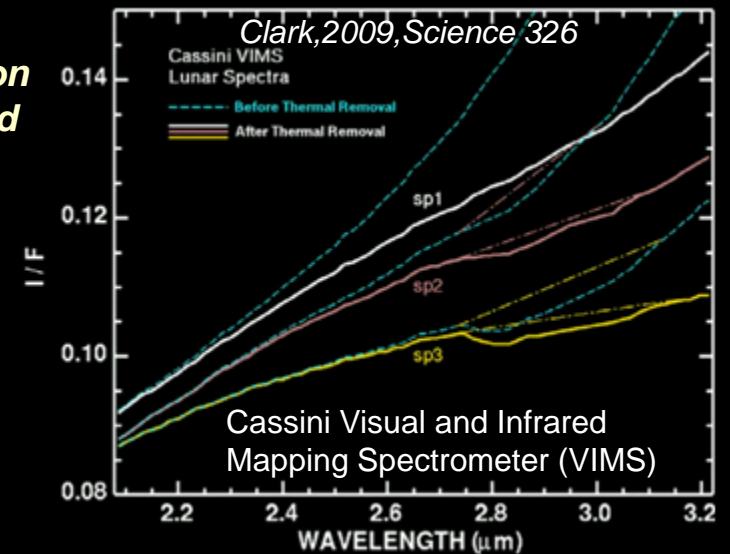
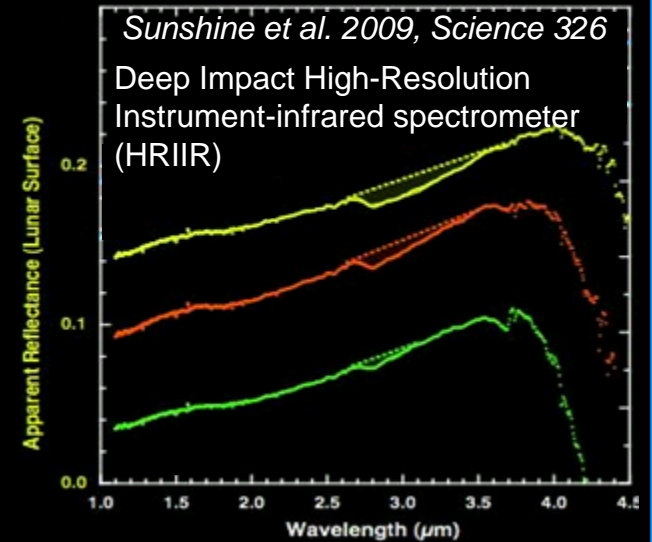


Fig. 2. Scaled reflectance. The 3- μm absorption is informative of physical state of water and hydroxyl. Adsorbed water and hydroxyl, and internal hydroxyl are distinct from bulk liquid water (model derived from optical constants) and ice (not shown, but with absorption band centered near 3.07- μm). The absorption minimum of adsorbed water on the basalt lunar analog JSC-1A is at a shorter wavelength than for bulk water and longer than for hydroxyl. Internal hydroxyl and adsorbed hydroxyl are spectrally similar. The JSC-1A spectra have been scaled by the same factor. Upon heating the JSC-1A under vacuum to 388 K, the depth of the band decreased $\sim 50\%$, but the shape remained constant.

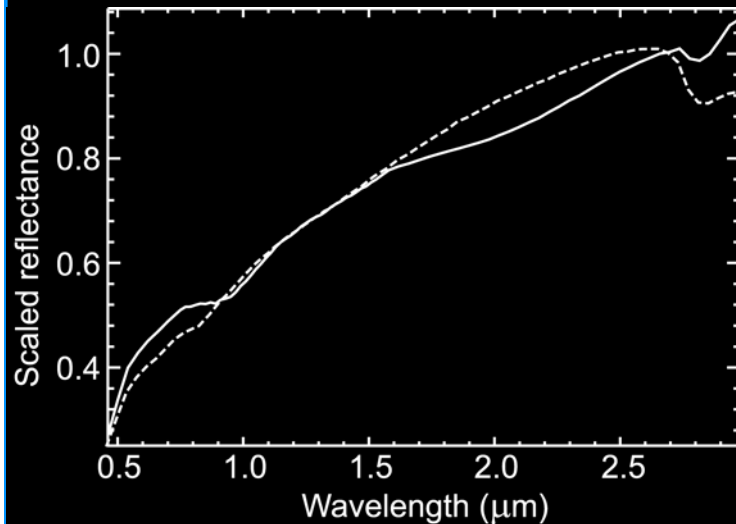


→ First detection of OH on the Moon by near-infrared spectroscopy

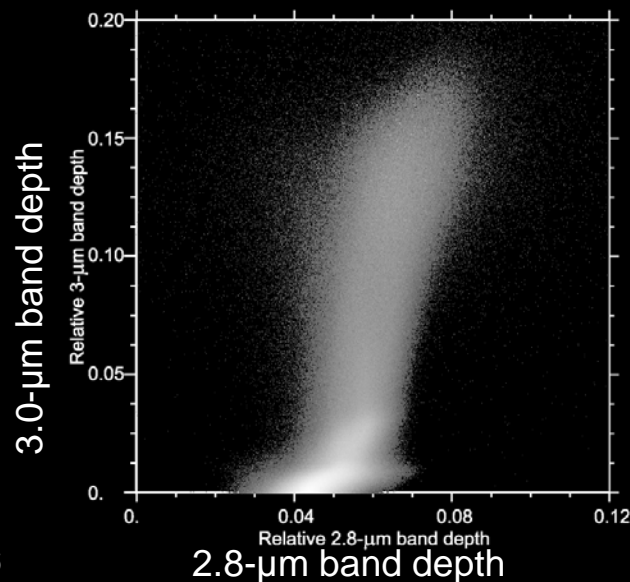
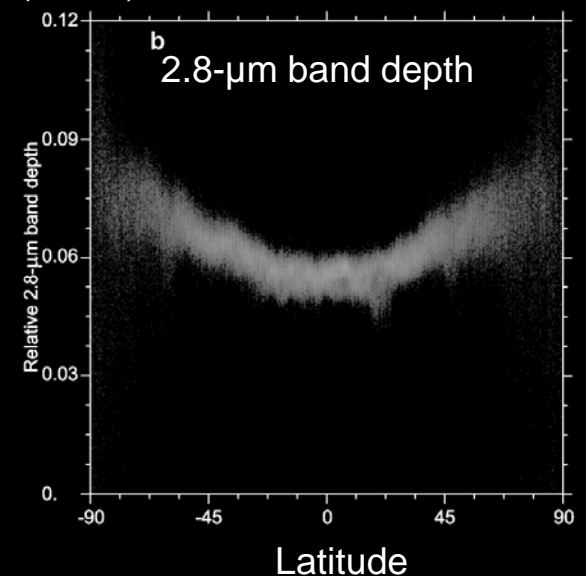
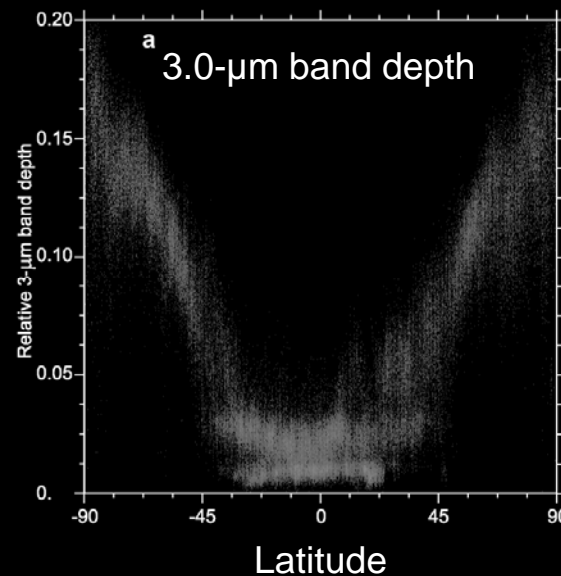


Distribution of Lunar OH/H₂O

Possible Distinction Between OH/H₂O in the Near-Infrared



Absorption band analysis from M³ near-infrared spectroscopy
McCord et al., 2011, JGR 116



Possible different spectral character:
2.8-μm band enhanced → OH
3.0-μm band enhanced → OH or H₂O

Diffuse, positive correlation of the two

→ **Distinction between OH and H₂O not yet formally demonstrated from M³ spectra**

DETECTION OF LUNAR H₂O FROM ULTRAVIOLET SPECTROSCOPY

Lyman-Alpha Mapping Project (LAMP)
Hendrix et al., 2012, JGR 117

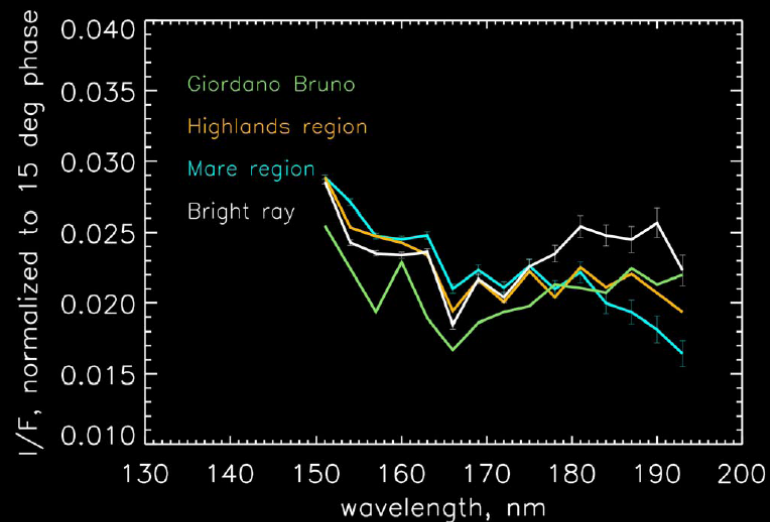


Figure 5. Sample LAMP reflectance spectra of a sample mare region, a sample highlands region and two “fresh” regions: a bright ray and the young Giordano Bruno crater for comparison. Representative statistical error bars are shown.

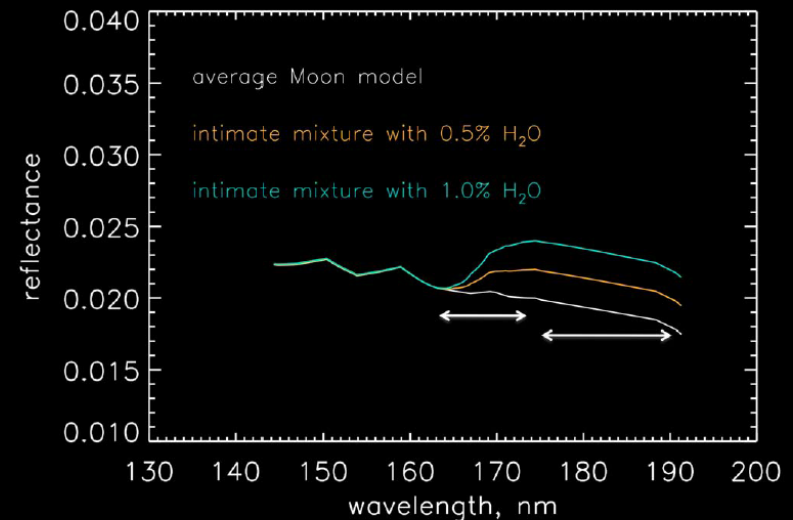


Figure 6. Intimate mixture models for average lunar terrains with varying amounts of water ice. The slope in the 164–173 nm range is expected to increase (redden) with increasing water content; the slope in the 175–190 nm range should be unaffected by H₂O content.

Distribution of Lunar OH/H₂O

Global Mapping of Lunar Elemental Hydrogen and OH/H₂O

Epithermal Neutron flux from Lunar Prospector
Litvak et al., 2012, JGR 117

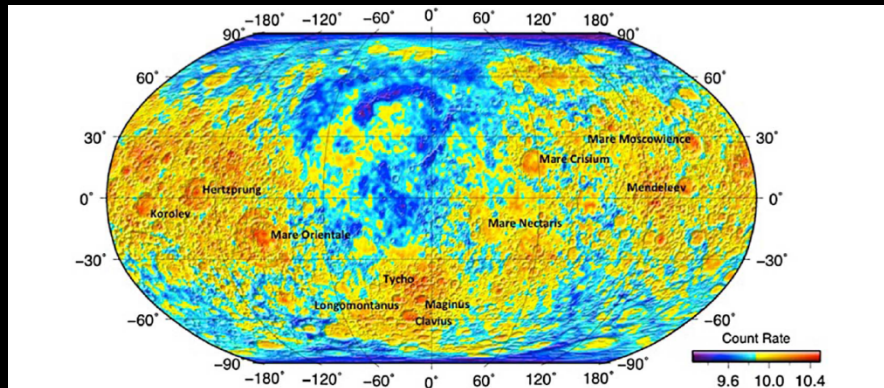
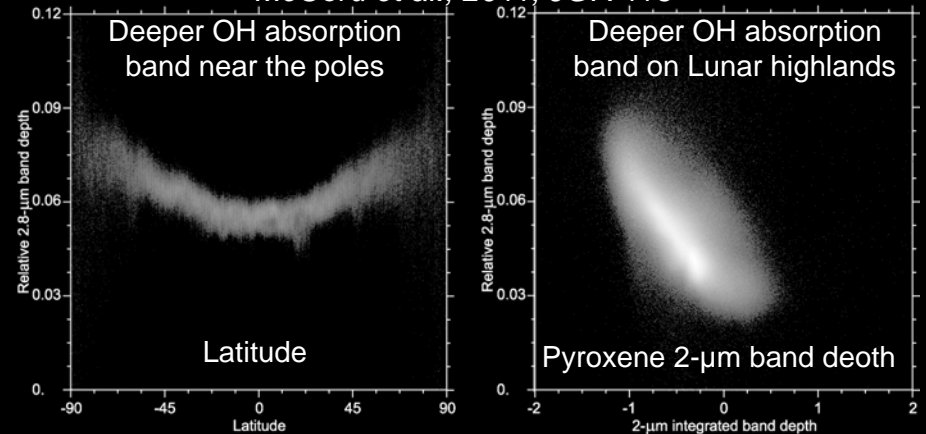


Figure 16. Smoothed (Gaussian filter with FWHM = 60 km) map (in Robinson projection) 1° × 1° of epithermal neutron counting rate (background subtracted, thermal neutron component removed, counts per second) measured in LEND SETN detector. The counting rate in SETN was corrected for the detector efficiency changes, long-term variations of GCRs. The counting rate was also reduced by the GCR spacecraft background (defined at the cruise) and by contribution of thermal neutron counting rate derived from equations (3) and (4).

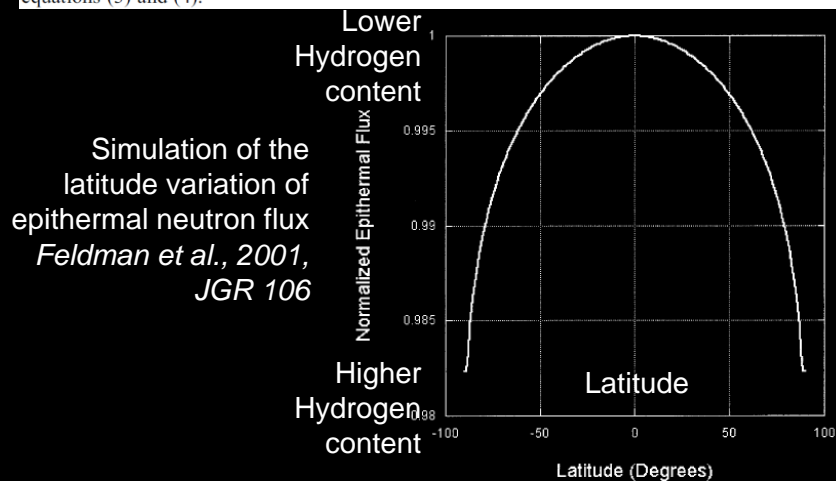
OH absorption band depth from M³ near-infrared spectroscopy
Clark et al., 2011, JGR 116



Absorption band analysis from M³ near-infrared spectroscopy
McCord et al., 2011, JGR 116



→ **Enhancement of volatile content at the poles consistent between neutron count and near-infrared spectroscopy**



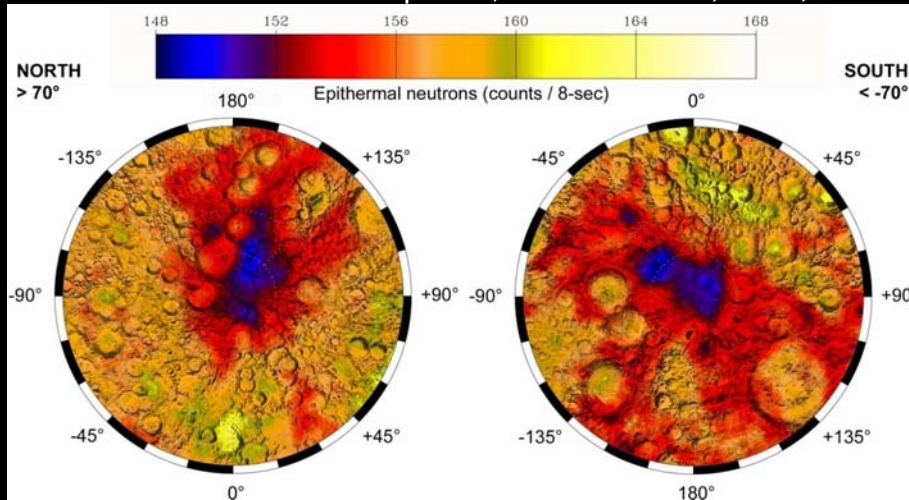
Simulation of the latitude variation of epithermal neutron flux
Feldman et al., 2001, JGR 106

Figure 3. Simulation of the latitude, λ , variation of epithermal neutron flux (normalized to the equator) under the assumption of a $\text{Cos}^{1/4} \lambda$ temperature dependence and a constant FAN composition.

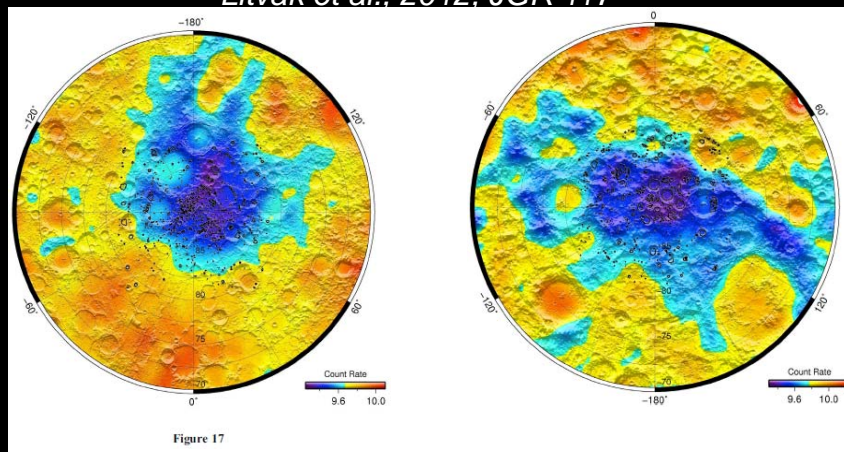
Distribution of Lunar OH/H₂O

Polar Mapping of Lunar Elemental Hydrogen

Neutron detector on Lunar Prospector, *Feldman et al., 2001, JGR 105*



Lunar Exploration Neutron Detector (LEND) on LRO
Litvak et al., 2012, JGR 117



Lunar Exploration Neutron Detector (LEND) on LRO
Mitrofanov et al., 2012, Science 330
Permanently shaded region (example of Cabeus)

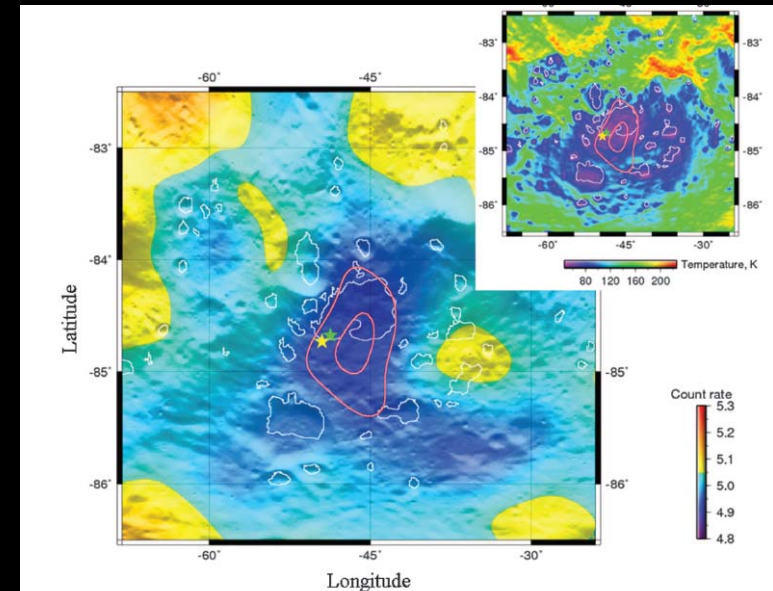


Fig. 1. LEND-derived map of the epithermal neutron flux within Cabeus crater (primary cavity). Colors represent the level of epithermal neutron flux (cps). The map is smoothed by a Gaussian filter with a 14-km scale (1 σ). The thin white contours outline the boundaries of PSRs according to best-available LOLA altimetry. The outermost pink contour represents the statistically most likely boundary of the NSR within the Cabeus crater, and the innermost pink contour represents the region of strongest neutron suppression within the NSR (Cases 10 and 11 of Table 1, respectively, and SOM, section 5). The colored stars represent the locations of the LCROSS impact sites (green and yellow correspond to the Shepherding Spacecraft and the Centaur upper stage, respectively). The insert (upper right) represents the map of subsurface temperatures within Cabeus from the LRO Diviner instrument (17); the contours associated with the LOLA-defined PSRs and LEND-defined NSR are also shown on this inset temperature map (upper right).

→ **Enhancement of elemental hydrogen at the poles confirmed by measurements from two instruments**
→ **Maximum Hydrogen content in permanently shaded regions**

Distribution of Lunar OH/H₂O

SEARCH FOR OH/H₂O IN PERMANENTLY SHADOWED REGIONS

Detection of water from an impact plume

Colaprete et al., 2010, Science 330

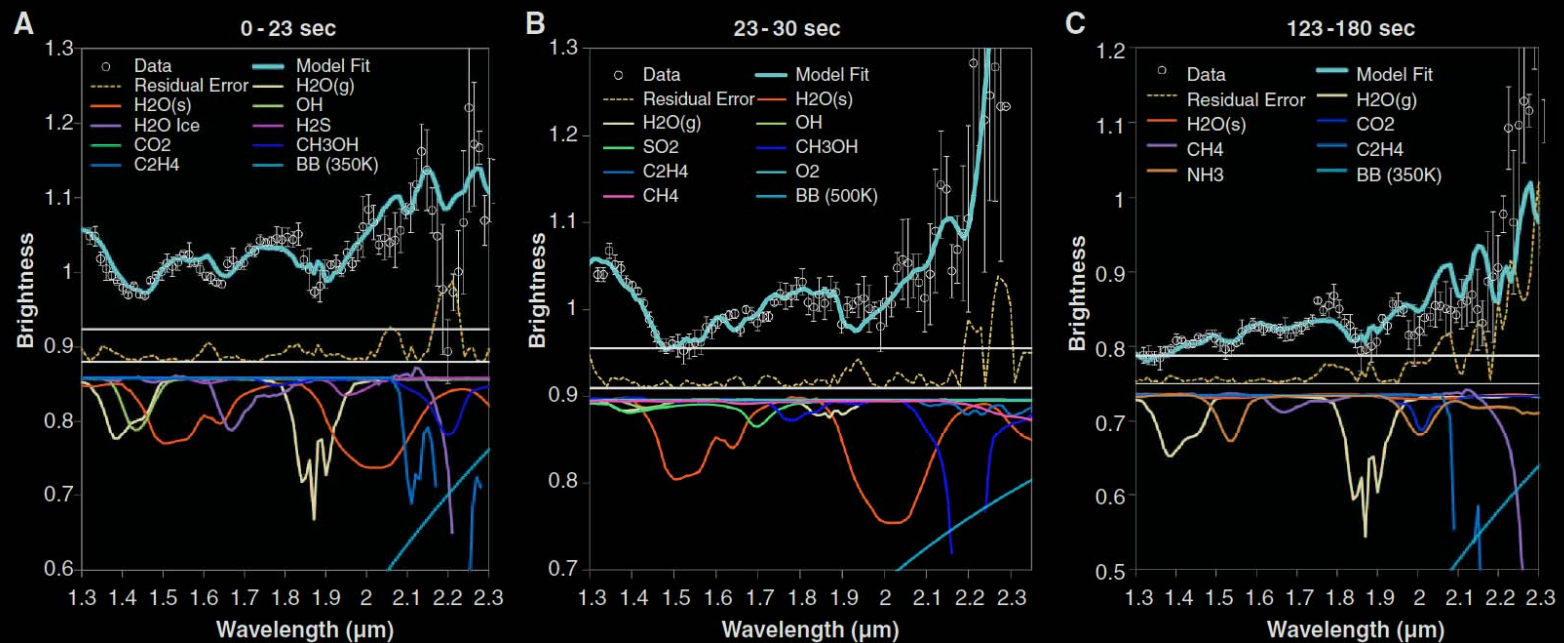


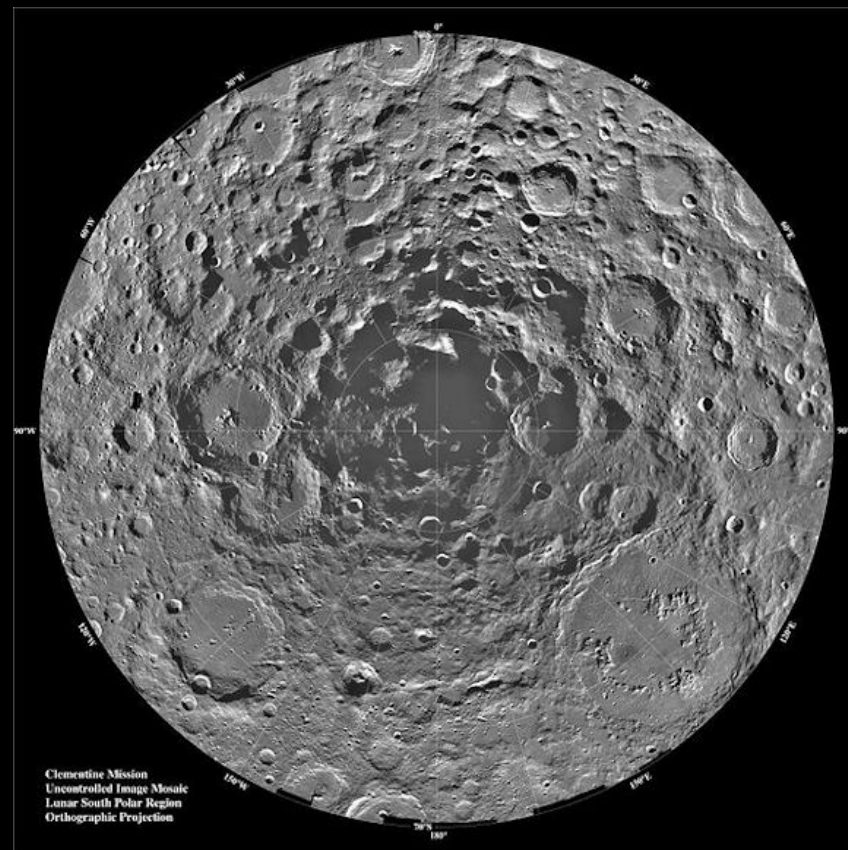
Fig. 3. (A to C) Model fits to the NIR reflectance spectra for three periods after impact. The measured spectral reflectance is shown with 1 SD error bars (measurement variance for the average of ~90 spectra). The fit ("Model Fit") was produced using the various volatiles indicated by the curves (each curve is normalized to water ice to show relative abundances with respect to each other) at the lower part of each figure [H₂O(g) and H₂O(s) are water vapor and water ice, respectively]. Water vapor fluo-

rescent emission is provided as a possible contribution but is not found to be necessary to fit the data within the uncertainty of the measurements. The total residual error between the observation and the model is shown (dark blue dashed line) and the 5% level indicated by a solid black line. In the wavelength range between 1.3 and 2.0 μm, residual error is typically <1.5%. The χ^2/ν for each of the three fits is 1.16, 1.8, and 1.2, respectively.

Distribution of Lunar OH/H₂O

LIMITATIONS FOR POLAR MAPPING OF LUNAR OH/H₂O

In deeply shaded areas:
lack of solar illumination for
accurate mapping with current
dataset from spectrometers



LUNAR OH/H₂O

Variations

Investigations of temporal variations

- EPOXI (*Sunshine et al., Science, 2009*)
- M³ (*Pieters et al., 2009, Science 326 ; McCord et al., 2011, JGR 116*)
- LAMP (*Hendrix et al., 2012, JGR, 117*)

Limitations in the interpretation of these variations

- Thermal emission
- Photometry

Variations of signal sensitive to OH/H₂O

NIR INVESTIGATIONS OF TEMPORAL VARIATIONS OF LUNAR OH/H₂O

Possible variation of the 2.8- μ m absorption band with time of day

Sunshine et al., 2009, Science 326

McCord et al. 2011, JGR 116

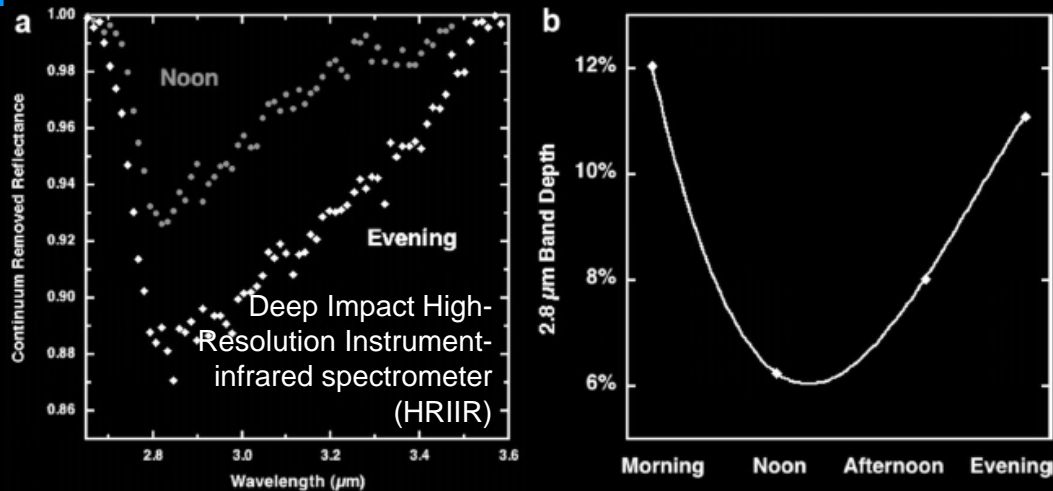


Figure 17. Examples of EPOXI observations of the 3 μ m absorption for a lunar highlands region at different times of the lunar day. (a) The absorption has been isolated by removing a straight-line continuum fitted at each end of the absorption. (b) The band strength appears to vary and is strongest at lowest lighting.

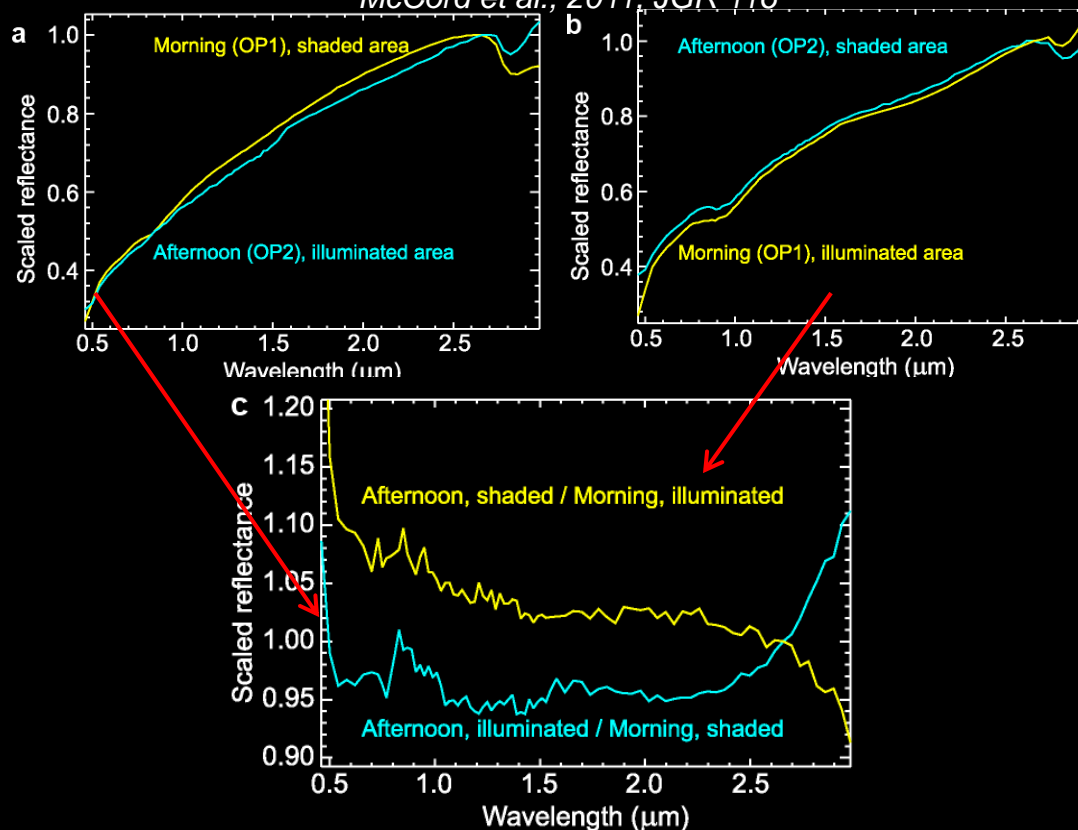
→ Possible temporal variations of the 3- μ m band depth

Variations of signal sensitive to OH/H₂O

EFFECTS OF THERMAL EMISSION ON THE DETECTION OF LUNAR OH/H₂O

Domination by thermal emission

Absorption band analysis from M³ near-infrared spectroscopy
McCord et al., 2011, JGR 116

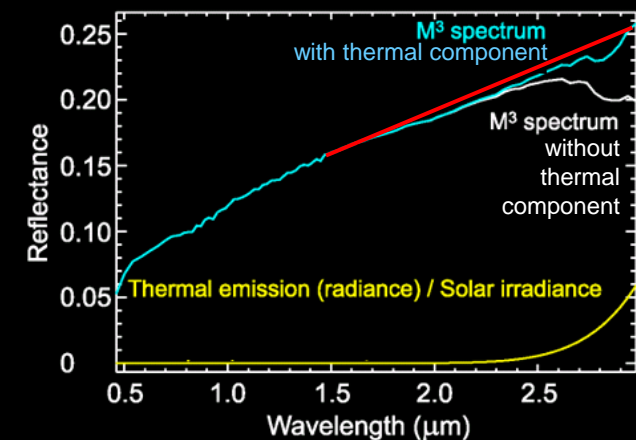


→ *The shape of these ratios is consistent with differences in thermal emission contributions*

Thermal emission correction of M³ data:
Extrapolation of a linear continuum

Method designed to not overcorrect the thermal contribution

$$R_o' = R_o + d_o^2 B_o(e, T) / F_{\text{sun}}$$



Method described in:
Clark, 1979, Icarus 40
and in *Clark et al., 2011 JGR 116*

The 3-μm absorption compensates the thermal emission

- **Underestimation of the thermal contribution**
- **Limitation of the detectability of temporal variations from M³ data**

Variations of signal sensitive to OH/H₂O

NIR INVESTIGATIONS OF TEMPORAL VARIATIONS OF LUNAR OH/H₂O

Possible variation of the 2.8- μ m absorption band with time of day

Sunshine et al., 2009, Science 326

McCord et al. 2011, JGR 116

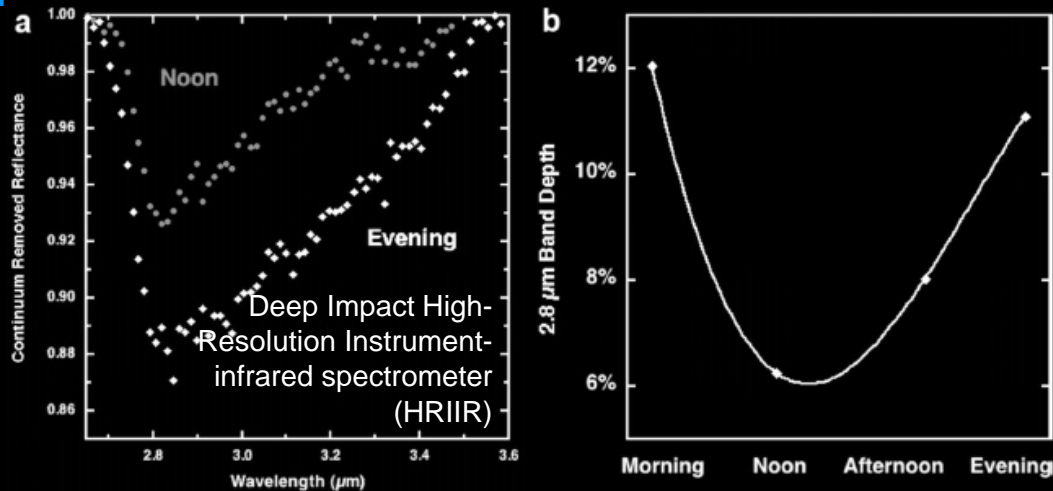


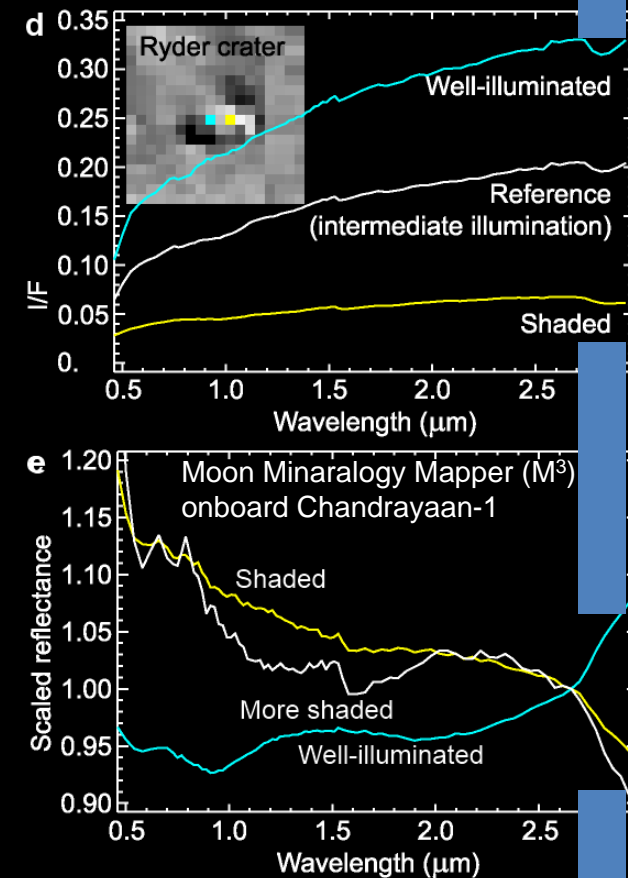
Figure 17. Examples of EPOXI observations of the 3 μ m absorption for a lunar highlands region at different times of the lunar day. (a) The absorption has been isolated by removing a straight-line continuum fitted at each end of the absorption. (b) The band strength appears to vary and is strongest at lowest lighting.

Deep Impact: Variations of the 2.8- μ m band depth
M³: Kink at 2.7 μ m in the ratio at crater Ryder

→ Possible indication of temporal variations of the 3- μ m band depth

Possible variation of the 2.8- μ m absorption band with varying illumination across Ryder crater

McCord et al. 2011, JGR 116



Variations of signal sensitive to OH/H₂O

UV INVESTIGATIONS OF TEMPORAL VARIATIONS OF LUNAR OH/H₂O

LAMP spectra on Lunar Reconnaissance Orbiter

Hendrix et al. 2012, JGR 117

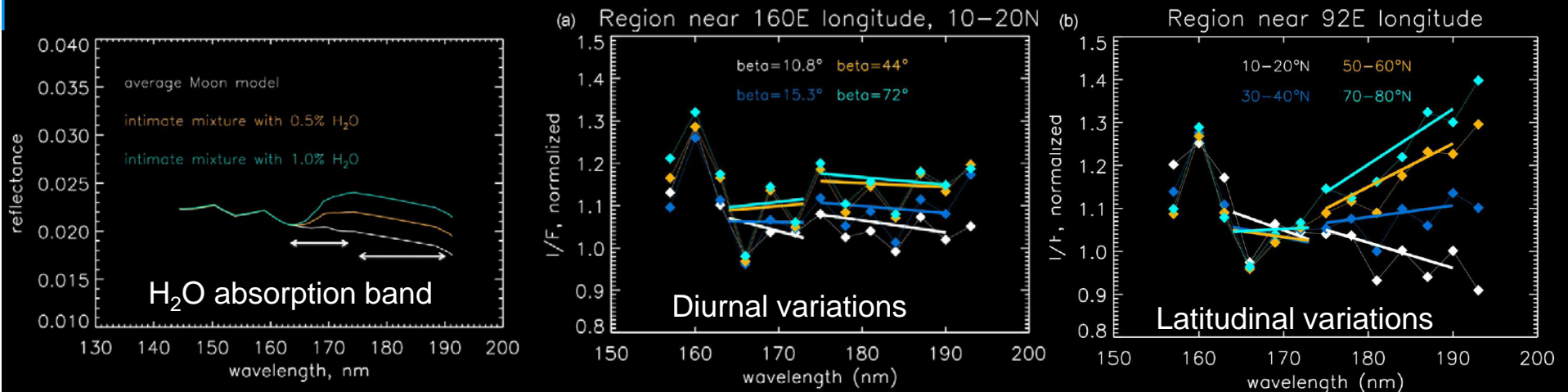


Figure 6. Intimate mixture models for average lunar terrains with varying amounts of water ice. The slope in the 164–173 nm range is expected to increase (redden) with increasing water content; the slope in the 175–190 nm range should be unaffected by H₂O content.

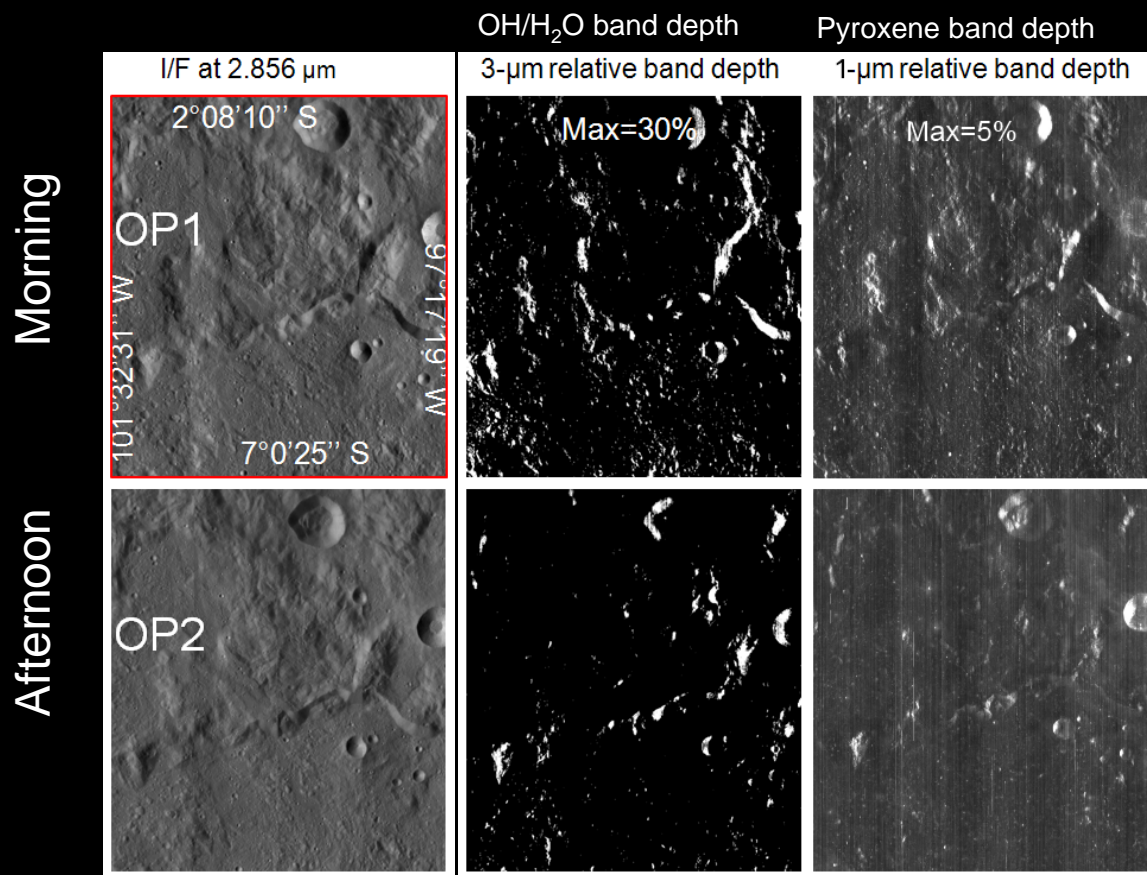
Figure 9. Reflectance spectra (normalized) of (a) a region on the lunar farside near 160°E at 4 different beta angles and (b) a longitude band near 92°E at 4 different latitudes, from March 23 2010 orbits when the beta angle was ~6°. The slopes in both wavelength ranges increase with latitude; this is particularly obvious at the longer wavelengths for the normalization used here. The slope increases with beta angle only in the 164–173 nm range, suggesting a diurnally variable composition related to H₂O.

→ Possible variations of the content in H₂O with illumination

Variations of signal sensitive to OH/H₂O

EFFECTS OF SURFACE PHOTOMETRY ON THE DETECTION OF LUNAR OH/H₂O

M³ near-infrared spectroscopy
McCord et al., 2011, JGR 116



Absorption band depth is sensitive to the geometry of illumination and observation

Multiple-scattering enhances the depth of absorption bands

- **Photometry is a limitation factor in the detection of temporal variations**
- **Needs to be combined with a more accurate thermal emission correction**

Variations of signal sensitive to OH/H₂O

LIMITATIONS FOR MONITORING TEMPORAL VARIATIONS OF ELEMENTAL HYDROGEN

Neutron flux must be integrated over long periods of times

→Lack of flux and spatial resolution for time-dependance monitoring

Neutron detectors integrate flux from the first meter below the subsurface

→ Any variations may be smoothed out

LUNAR OH/H₂O

Origins

Implantation of protons from the solar wind

Meteorites and comets

Endogenic

WHAT THE MODELS HAVE TO EXPLAIN

Summary of the observations:

Presence of elemental Hydrogen in the first meter of the regolith

Presence of OH and possibly H₂O in the first millimeters of the regolith

Enhanced contents of Hydrogen and OH toward the poles and in permanently shaded regions

Possible OH content variability as function of local time of day and solar illumination

Possible variations as function of the mineral composition

None of the models for the origin or delivery account for the observed distribution of elemental Hydrogen and OH/H₂O
→ After delivery on the surface, the observed volatiles have to be mobile

Models for the origin of volatiles

- Accretion (endogenic origin of volatiles of
- Delivery (comets, meteorites)
- Creation (implantation of protons from the solar wind)

Models for the mobility of volatiles

- Chemical stability of H₂O in lunar materials and lateral transport from low latitudes to permanently cold areas
- Vertical transport from the surface to the subsurface for long-term preservation

Crider & Vondrak, 2000, JGR 102

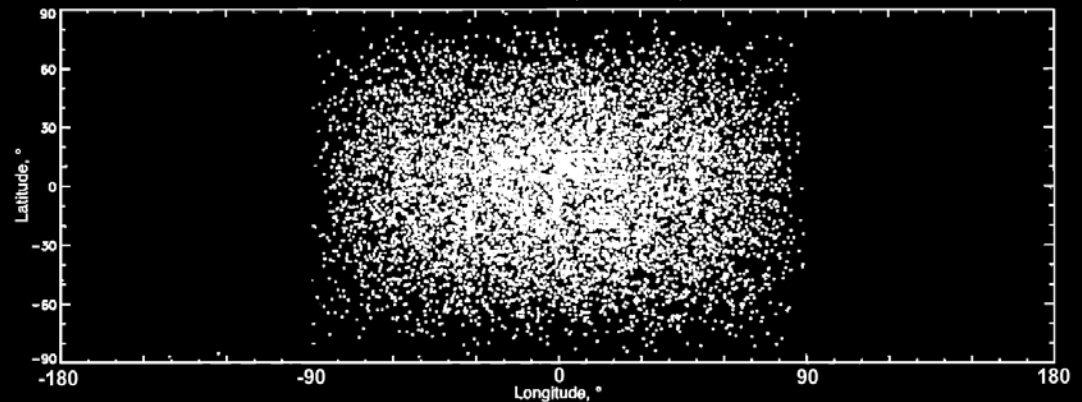


Figure 2. Distribution in latitude and longitude of 10,000 particles from a source function like the solar wind. The subsolar point is at [0, 0].

Origins of Lunar OH/H₂O

IMPLANTATION OF PROTONS FROM THE SOLAR WIND

Damaged molecular bonds from micrometeorite bombardment
 → Dangling O⁻ bonds

Implantation of protons from the solar wind
 → Formation of -OH
 (Zeller et al., 1966, JGR 71)

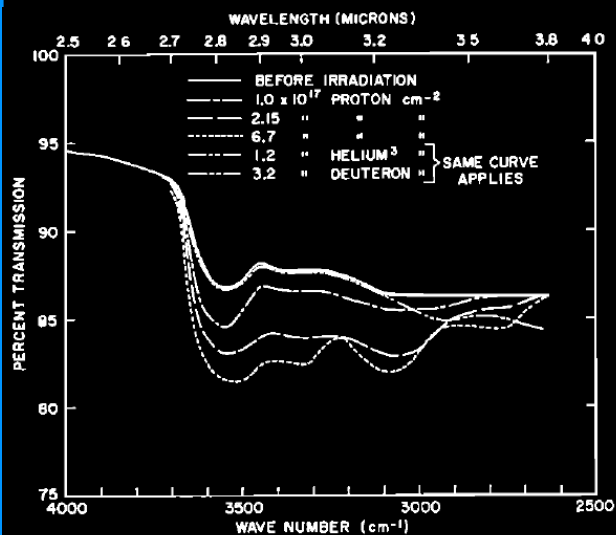


Fig. 1. Infrared absorption spectrum of a silicate glass plate before and after the indicated irradiations.

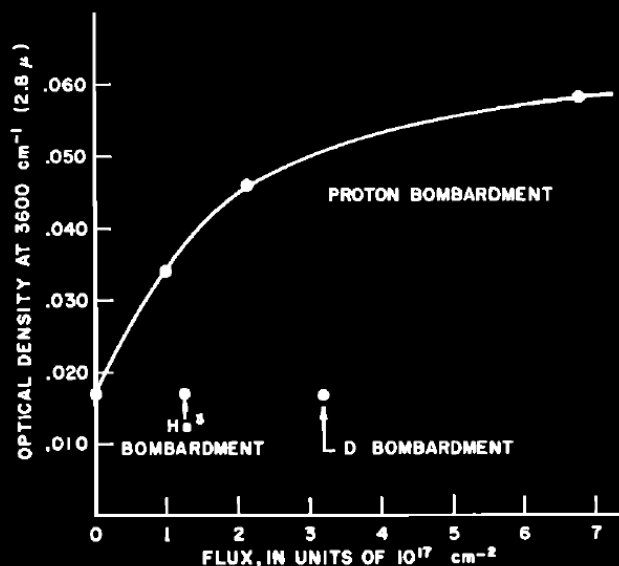


Fig. 2. Optical density, i.e., the magnitude of absorption of the OH stretching mode at 2.8 μ, before irradiation and after the various irradiations listed in Figure 1.

McCord et al., 2011, JGR, 116

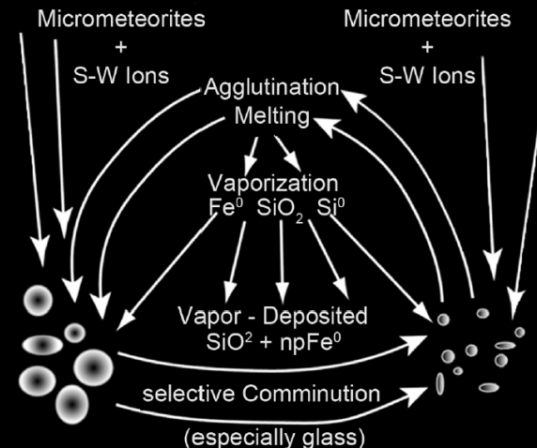
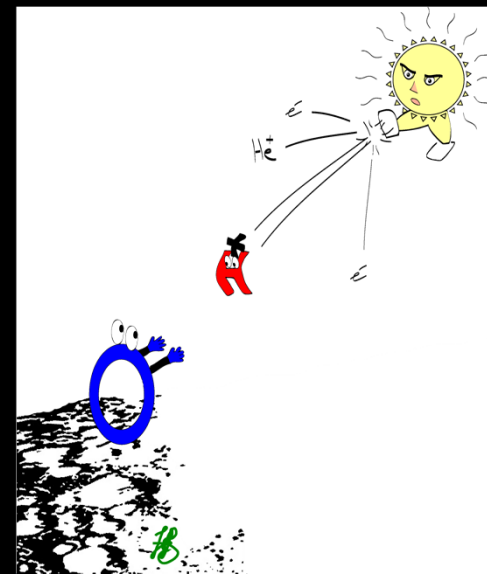


Figure 2. An illustration of some of the chemistry the solar wind ions and micrometeoroids enable in the lunar surface grains.

McCord & Combe, 2011, LPSC 1493



Further investigation, models and experiments:
 Starukhina et al., 2000, 2001, 2006
 Strazulla et al., 2005

Origins of Lunar OH/H₂O

OH/H₂O ON MAGNETIC ANOMALIES

Examples of lunar swirls

M³ near-infrared spectroscopy
Kramer et al., 2011, JGR 116

Lunar crustal magnetic field anomalies from Lunar Prospector (*Kramer et al., 2011, JGR 116*
Adapted from Halekas, 2003, PhD thesis)

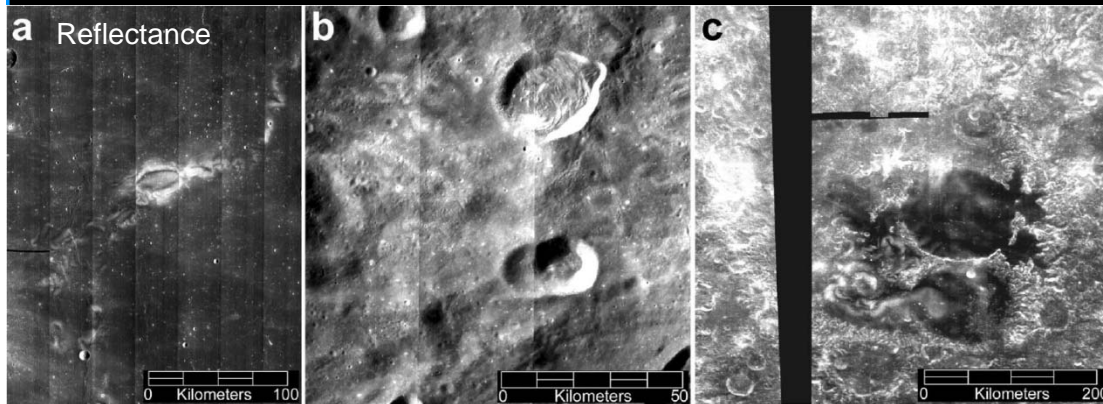


Figure 2. M³ mosaics of the three regions selected for this study shown in true color (R = 700 nm, G = 580 nm, B = 460 nm). (a) Reiner Gamma, (b) Gerasimovich, and (c) Mare Ingenii.

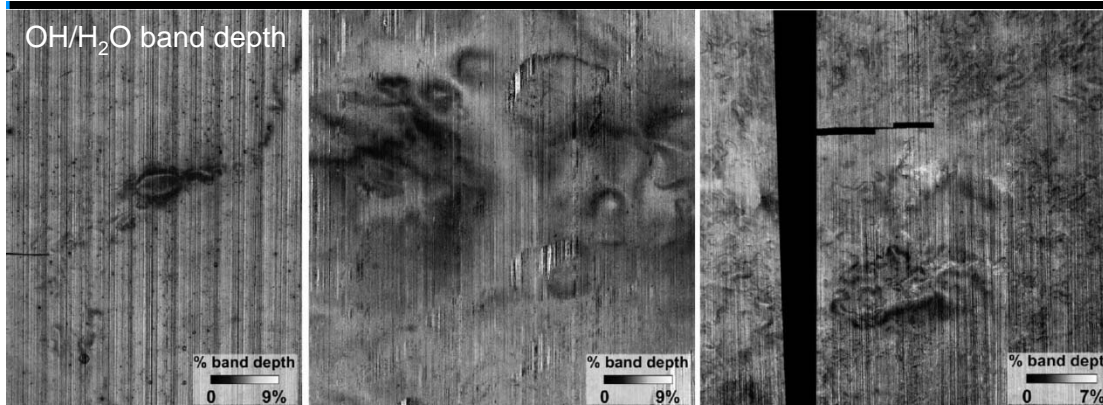
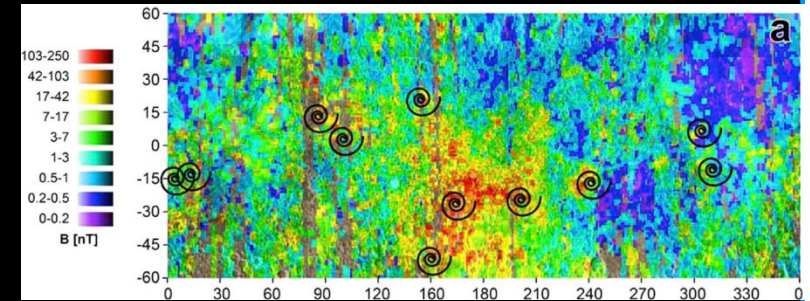


Figure 4. Parameter image of the depth of the 2.82 μm absorption feature, calculated as the percent difference in albedo from a straight-line continuum. This parameter shows the relative hydroxyl (OH) abundance of the three studied swirl regions: (a) Reiner Gamma, (b) Gerasimovich, and (c) Mare Ingenii. The swirls are recognizable by their shape and low OH abundance.



Link between surface hydroxyl formation, optical maturation at magnetic anomalies and swirls

→ **Pattern consistent with crustal magnetic anomalies creating variations of the flux of solar wind protons at the surface**

Origins of Lunar OH/H₂O

INFALL OF VOLATILE-RICH METEORITES

AND COMETS

Recent impact of a comet or asteroid onto the lunar surface

Shevchenko, 1999;

Klumov and Berezhnoi, 2002;

Lunar swirls:

Schultz and Srnka, 1980;

Pinet et al., 2000;

Starukhina and Shkuratov, 2004

Possible retention of water through comet or meteorite impact mechanisms

Ong et al., 2010, Icarus 207

Example of Vesta:

→ Evidence for major contribution by infalling volatile-rich meteorites (although in a different environment of the solar system)

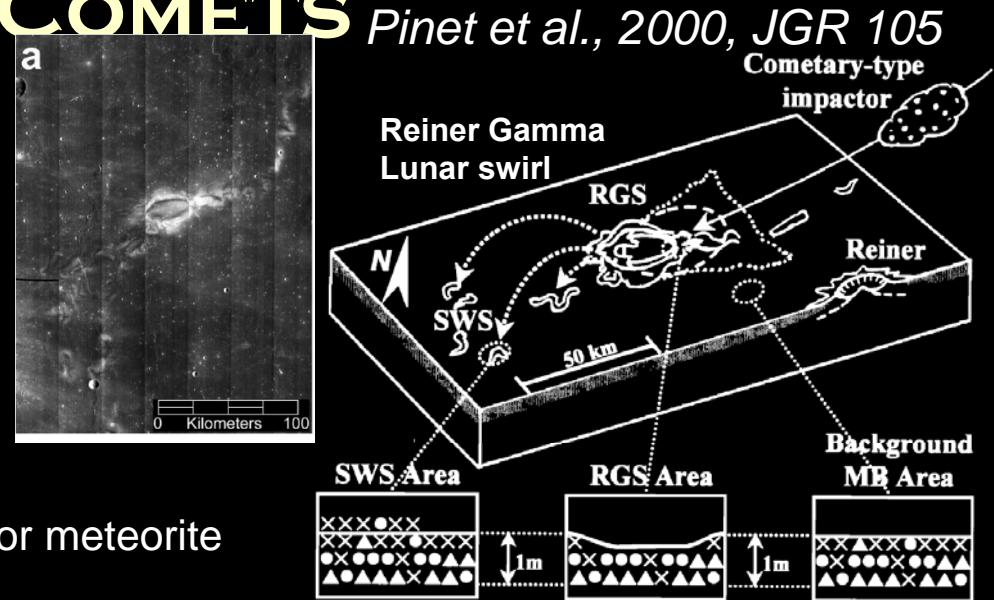


Figure 4. Sketch of the disturbing effects in the regolithic near-surface layer (depth of the order of 1 m) caused by an oblique impact of a cometary low-density body and accounting for the observed optical modifications. Shown is the upper layer of the typical mare soil: crosses refer to the fine fraction of the mare soil with diameter $\varnothing < 45 \mu\text{m}$; solid circles refer to the size fraction with $45 < \varnothing < 94 \mu\text{m}$; and solid triangles refer to the coarse size fraction $> 95 \mu\text{m}$. Physical characteristics (size fraction distribution and modification of the soil layering) of the regolith layer at the RGS, SWS, and MB sites are sketched in the corresponding cross sections. MB refers to the undisturbed mare background situation; RGS corresponds to a relative depletion of the fine fraction and correlative enrichment of the 45-94 μm size fraction; and SWS shows a relative fine fraction enrichment by the deposition of the fine fraction transported by a wind-like-type effect (see text). Dashed circle indicates the extent of the zone where the fine fraction is prevalently removed, as typified by RGS end-member and related cross section. Dotted triangular contour demarcates the extent of the zone where the mare regolith is modified. It corresponds spatially to the red halo unit (see Figure 2i), modeled by a combination of 20-40% of the SWS end-member mixed with 60-80% of the MB end-member (see Plates 3b and 3c).

Origins of Lunar OH/H₂O

OH/H₂O BROUGHT BY ACCRETION DURING THE FORMATION OF THE MOON

First detection of water in lunar samples
→ Concentration profile from grain core
to rim suggests endogenic origin and
possible outgassing
(Saal *et al.*, 2008, *Nature*)

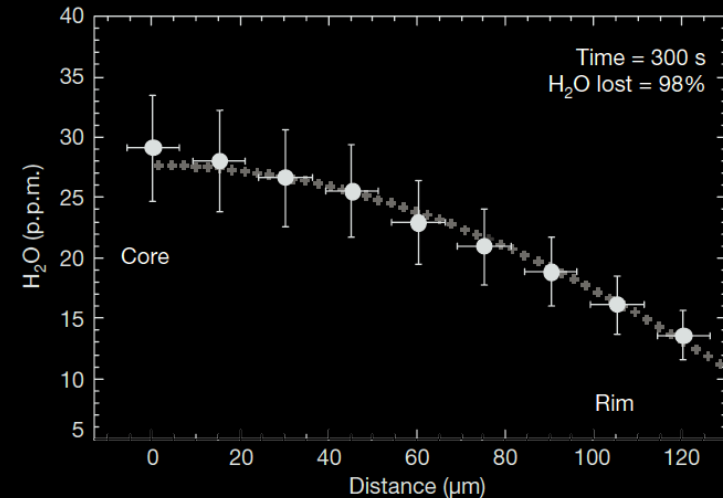


Figure 2 | Volatile concentration profiles from core to rim in a single bead of the very-low-Ti glasses. The glass used is 'Green #5' (see Supplementary Tables 1 and 4). The black filled circles represent the measured profiles, the grey filled crosses define the output data of the model describing the diffusive volatile loss from a homogeneous sphere with concomitant surface evaporation; see text for details and Supplementary Tables 4 and 5 (Case 1) for model parameters. Error bars represent standard deviation (2σ) uncertainties, and the size of the rastered ion beam. Volatile contents are in parts per million. To avoid any possible influence of ions implanted by solar wind, we did not analyse the outermost rim of the glass bead; the measured concentration profiles stop 18 μm before reaching the rim of the bead. The sharp decrease in volatile content from core to rim for H₂O, Cl, F and S suggests that the volatile contents are indigenous to the Moon and were affected by degassing during magma eruption. As expected, H₂O has the largest observed variation from core to rim, followed by Cl, F and S, indicating progressively less degassing for those elements, respectively.

LUNAR OH/H₂O ORIGIN AND DELIVERY

Implantation of protons from the solar wind

Meteorites and comets

Endogenic

→ All mechanisms for the origin and delivery may contribute

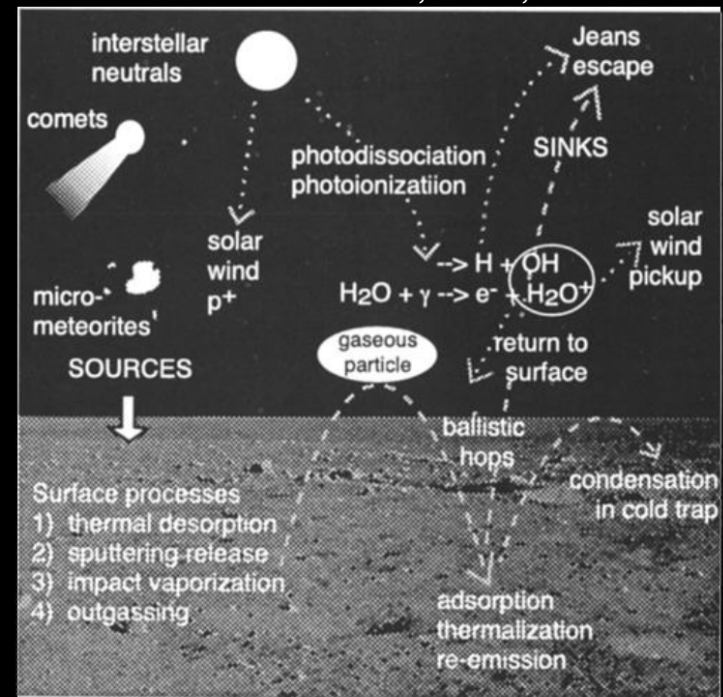
LUNAR OH/H₂O

Mobility

Crider & Vondrak, 2000, JGR 102

Lateral transport from low latitudes to permanently cold areas by **adsorption and desorption** mechanisms of H₂O onto/from lunar materials combined with ballistic trajectories

Vertical transport fro the surface to the subsurface for long-term preservation



Background photo from NASA NSSDC, Apollo 11 landing site

Figure 1. The process involved with the migration and retention of volatiles to the lunar polar cold traps.

Mobility of Lunar OH/H₂O

STABILITY OF LUNAR OH/H₂O IN AR MATERIALS

Hibbitts et al 2011 *Icarus* 213

- Adsorbed hydroxyl more stable than water

- Low latitudes hydroxyl may become mobile and recombinatively desorb as water

→ one explanation for the observed diurnal variation in the depth of 2.8- μ m feature at low latitudes

→ consistent with the lack of lunar water in returned Apollo samples.

- Desorbed water → accumulates in cooler areas if not dissociated by other processes.

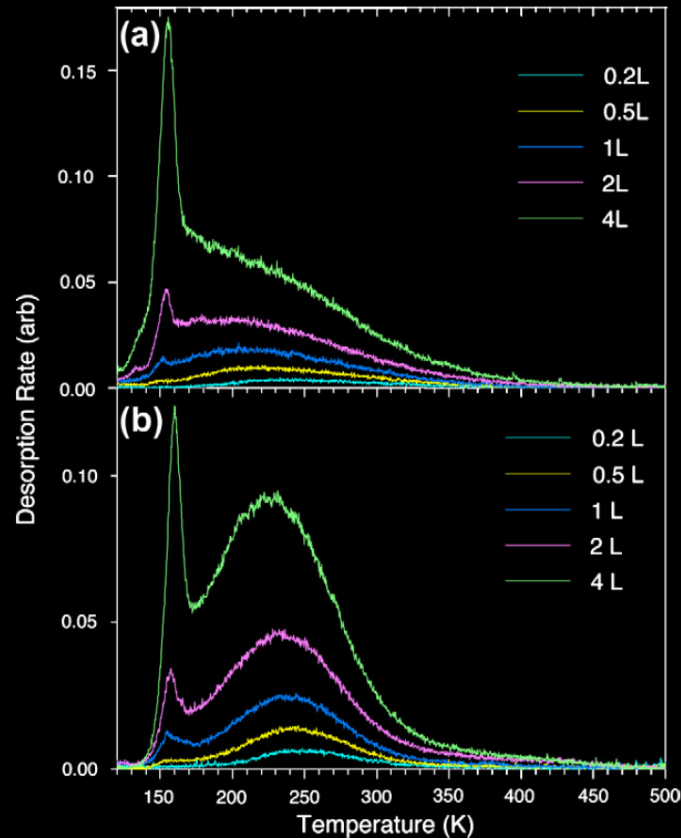
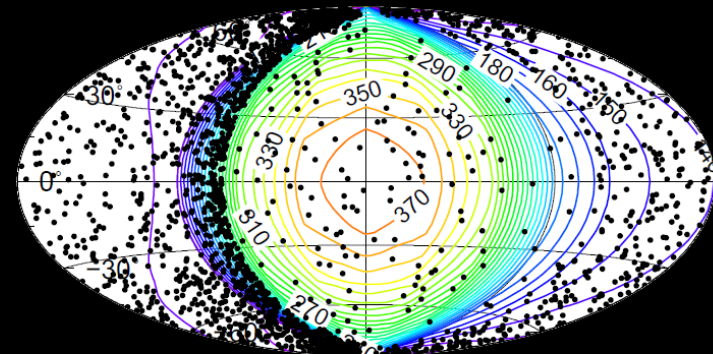


Fig. 4. Thermal desorption curves of water from (a) JSC-1A and (b) albite. Dosing occurred at 110 K. Adsorbed H₂O chemisorbs at low exposure and remains present to ~400 K. Water clusters begin to form at exposures of 1 L or more. A water ice peak occurs ~170 K, chemisorbed waters desorb at higher temperatures. Albite is more adsorbing than JSC-1A with chemisorbed water dominating over ice desorption at larger exposures.



Schorghofer, 2012, *LPSC 1110*

Figure 2: Steady-state distribution of water molecules on a global map (equal-area Hammer projection). There is an enhanced concentration of water molecules near the morning terminator, but not at the evening terminator. Colored contours are surface temperature with noon at the center. The morning terminator is to the left of the center.

Mobility of Lunar OH/H₂O

LATERAL MIGRATION OF H₂O TO LUNAR COI

Schott et al., 2012, LPSC 1110

Waston et al., 1961, JGR 66 ; Arnold, 1979, JGR 84 ; Butler et al., 1997, JGR 102 ; Crider & Vondrak, 2000, JGR 102

Water molecules on the lunar surface move on ballistic trajectories until they reach one of the extremely cold permanently shaded areas near the lunar poles where they accumulate.

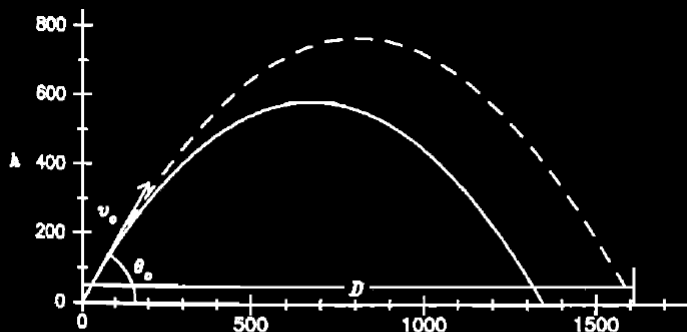


Figure 2. Molecule trajectories for cases where the gravity was assumed constant (solid line) and where the gravity was treated correctly, as in (6) (dashed line). Trajectories were calculated for Mercury, with an initial velocity of 2400 m/s, which was the approximate maximum velocity which occurred in the Monte Carlo simulations. The emergent angle θ_0 was 60° . Distances are in kilometers.

Butler et al., 1997, JGR 102

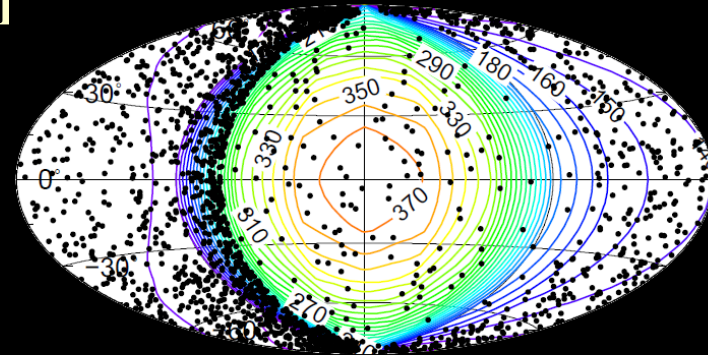


Figure 2: Steady-state distribution of water molecules on a global map (equal-area Hammer projection). There is an enhanced concentration of water molecules near the morning terminator, but not at the evening terminator. Colored contours are surface temperature with noon at the center. The morning terminator is to the left of the center.

Butler et al., 1997, JGR 102

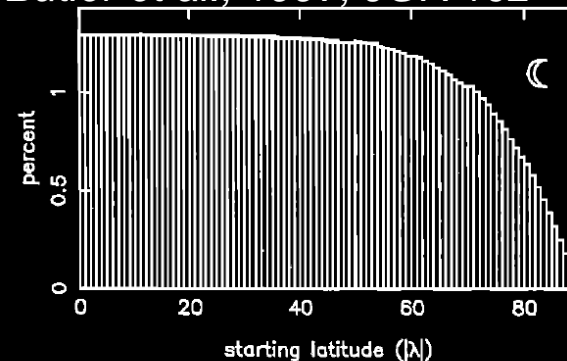


Figure 5. Histogram of the starting latitude of molecules which eventually became stable in the nominal Moon simulations, showing that equatorial molecules may become stable.

Mobility of Lunar OH/H₂O

VERTICAL MIGRATION OF H₂O AT LUNAR PERMANENTLY COLD AREAS

Schorghofer and Taylor, 2007, JGR 112

H₂O delivered on permanently cold areas

→ Two ways of accumulating H₂O ice in the subsurface

1- Diffusive migration to the subsurface

2- Pumping by diurnal temperature oscillations

Transport with partial or multiple molecular layers

Survival time of ice buried beneath porous regolith

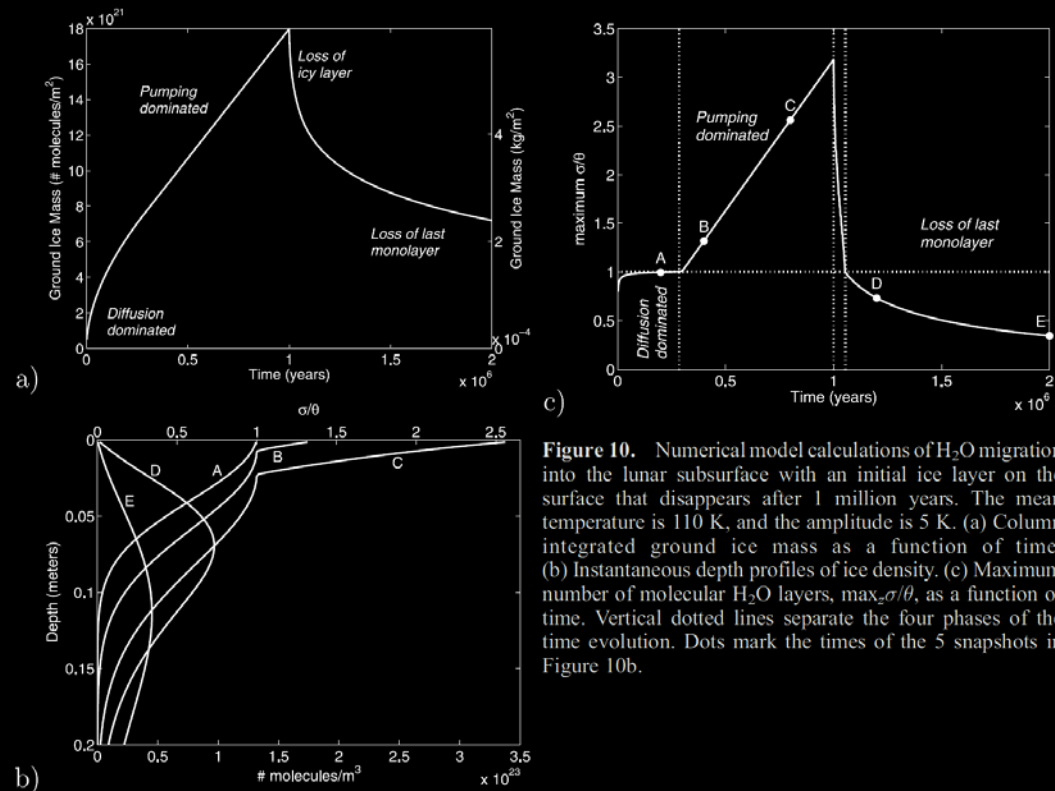


Figure 10. Numerical model calculations of H₂O migration into the lunar subsurface with an initial ice layer on the surface that disappears after 1 million years. The mean temperature is 110 K, and the amplitude is 5 K. (a) Column integrated ground ice mass as a function of time. (b) Instantaneous depth profiles of ice density. (c) Maximum number of molecular H₂O layers, max_zσ/θ, as a function of time. Vertical dotted lines separate the four phases of the time evolution. Dots mark the times of the 5 snapshots in Figure 10b.

SUMMARY

Distribution

Higher content of volatiles at higher latitudes

More OH/H₂O associated to highlands (according to UV and NIR spectroscopy)

Detection of H₂O at permanently shaded regions

Observed signal variations ≠ mobility of volatiles

Elemental hydrogen from epithermal neutron → Not enough data

OH/H₂O from reflectance in the UV and NIR → Possible, although not fully demonstrated yet (limitations from residuals of thermal emission and photometry)

Origins & Delivery mechanisms: All may exist

Endogenic: from lunar samples → Probably not enough to explain the surficial OH/H₂O

Comets & meteorites → May explain the observed amount of OH/H₂O

Proton implantation from the solar wind → Consistent with space weathering and lunar swirls

Mobility, following the delivery of volatiles at the surface

Necessary to explain the observed enhancement of H, OH/H₂O towards the poles

Retention/release mechanisms are chemically possible

Lateral mobility → From initial even distribution or point source to polar distribution

Vertical mobility → From surface deposits: Burial and long-term preservation

Scientific Motivations for Future Investigation of Lunar OH/H₂O

“Enable identification of lunar ice deposits at small (~100 m) spatial scales suitable for future extraction, sample analysis, and in-situ resource utilization.”

Scientific investigations:

- **Compositional state** (elemental, isotopic, mineralogic) and compositional distribution (lateral and depth) of the volatile component in lunar polar regions.
- **Source(s)** for lunar polar volatiles.
- **Transport, retention, alteration, and loss processes** that operate on volatile materials at permanently shaded lunar regions.
- **Polar regolith physical properties** (cold and possibly volatile rich).
- What the cold polar regolith reveals about the ancient solar environment.
- Determine the importance of polar volatiles **for the history of the solar system**
- **Tracking back the volatile flux** over the latter part of solar system history

Thank you for your attention...